High-power-load DCLM monochromator for a computed tomography program at BMIT at energies of 25–150 keV

Tomasz W. Wysokinski,[a]* Michel Renier,[b] Pekka Suortti,[c] George Belev,[d] Léo Rousset,[a] Madison Adam,[e] Denise Miller,[d] Norman Huber[f] and L. Dean Chapman[d]

[a]Science Projects, Canadian Light Source Inc., 44 Innovation Boulevard, Saskatoon, SK, Canada S7N 2V3, [b]European Synchrotron Radiation Facility, Grenoble, France, [c]Department of Physics, University of Helsinki, Helsinki, Finland, [d]Science Division, Canadian Light Source Inc., 44 Innovation Boulevard, Saskatoon, SK, Canada S7N 2V3, [e]Engineering Division, Canadian Light Source Inc., 44 Innovation Boulevard, Saskatoon, SK, Canada S7N 2V3, and [f]Huber Diffraktionstechnik GmbH and Co., Sommerstrasse 4, Rimsting 83253, Germany. *Correspondence e-mail: wysokinski@alumni.sfu.ca

The research program at the biomedical imaging facility requires a high-flux hard-X-ray monochromator that can also provide a wide beam. A wide energy range is needed for standard radiography, phase-contrast imaging, K-edge subtraction imaging and monochromatic beam therapy modalities. The double-crystal Laue monochromator, developed for the BioMedical Imaging and Therapy facility, is optimized for the imaging of medium- and large-scale samples at high energies with the resolution reaching 4 μm. A pair of 2 mm-thick Si(111) bent Laue-type crystals were used in fixed-exit beam mode with a 16 mm vertical beam offset and the first crystal water-cooled. The monochromator operates at energies from 25 to 150 keV, and the measured size of the beam is 189 mm (H) × 8.6 mm (V) at 55 m from the source. This paper presents our approach in developing a complete focusing model of the monochromator. The model uses mechanical properties of crystals and benders to obtain a finite-element analysis of the complete assembly. The modeling results are compared and calibrated with experimental measurements. Using the developed analysis, a rough estimate of the bending radius and virtual focus (image) position of the first crystal can be made, which is also the real source for the second crystal. On the other hand, by measuring the beam height in several points in the SOE-1 hutch, the virtual focus of the second crystal can be estimated. The focusing model was then calibrated with measured mechanical properties, the values for the force and torque applied to the crystals were corrected, and the actual operating parameters of the monochromator for fine-tuning were provided.

1. Introduction

A high-power-load double-crystal Laue monochromator (DCLM) has been constructed for computed tomography (CT) studies at the BioMedical Imaging and Therapy (BMIT) facility (Wysokinski *et al.*, 2007, 2015) located at the Canadian Light Source. A pair of bent Laue-type crystals were used, with the first crystal water-cooled. Design considerations for such monochromators are provided by, for example, Chukhovskii & Krisch (1992) and Suortti *et al.* (1994, 2001). Recent alternative designs are described by Renier *et al.* (2016) and Stevenson *et al.* (2017).

The objective of the monochromator operation is to expand the beam (increase the vertical divergence) and to increase the reflectivity as much as possible by bending the first crystal to the safe limit and then adjusting the bend of the second crystal
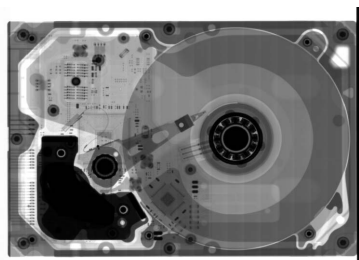
so that an elemental ray should make the same angle with the Bragg planes at both crystals. This will satisfy the condition for a non-dispersive crystal pair at all energies. Sometimes the goal is to generate a parallel (collimated) beam in the SOE-1 hutch; this can be very useful for commissioning activities and for dual-detector phase-contrast imaging tests at two sample-to-detector distances, although with decreased monochromaticity of the beam. BMIT's CT monochromator operates at energies from 31 keV to 150 keV with a 16 mm fixed beam offset, with the option of going down to 25 keV with extended offset. The monochromator was optimized for imaging large samples at high energy (80 keV), which requires a thick and wide crystal, in this case, 2 mm thick and 190 mm wide. To achieve the fixed beam offset, a pair of Si crystals with the same lattice spacing were used and the first crystal translates along the X-direction (along the direction of the beam) as the energy set-point changes. The second crystal is located at

Figure 1
Schematic of the 05ID-2 beamline.

a fixed position, 44.55 m from the source (see Figs. 1 and 7). The samples for imaging or therapy tests are positioned in the last hutch (SOE-1), which starts 6.7 m from the CT monochromator.
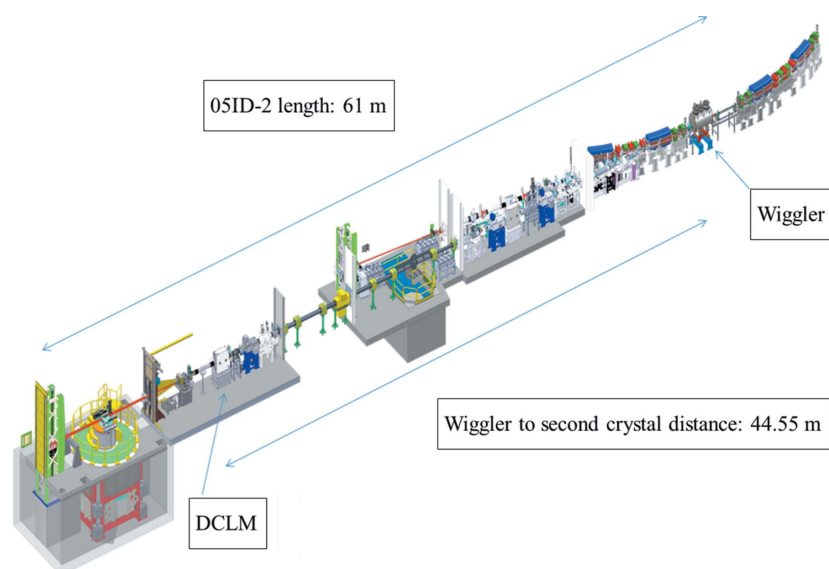
The total power of the BMIT wiggler (Wysokinski *et al.*, 2015; Wysokinski, Chapman *et al.*, 2016) is ∼14 kW at a 4.3 T field and 250 mA ring current. The high-power loads require a proper filter set to protect the crystal, reduce the outgassing and minimize thermal drift. The soft part of the wiggler spectrum causes most of the thermal effect, and for that reason ∼3 mm of C and ∼1 mm of Al are always used as filters to eliminate most of the spectrum below 20 keV.

2. DCLM overview and design criteria

2.1. Monochromator overview

There were no commercial monochromators available that met the beamline requirements at the time of construction of BMIT. The design team decided to develop a simplified version of the ID-17 monochromator from ESRF with the components water-cooled (Suortti *et al.*, 2000), and use standard stages as much as possible to reduce costs. The monochromator was allocated around 1.2 m of linear space in the optics hutch.

Each silicon crystal is attached to a tower made of two cradle stages (to define the Bragg and χ angles) plus one vertical stage to bring in and remove the crystal from the beam. In addition, the first crystal is attached to a linear stage which is required to keep the vertical beam offset fixed as the energy changes. A relatively simple vacuum chamber design was chosen to minimize the cost of the monochromator. Fig. 2 shows both the CAD model and a photograph of the monochromator set for 50 keV. Operation of the monochromator is

based on mechanical end-switch calibration only, since the use of encoders is not possible as a result of the high level of radiation inside the monochromator.

2.2. Crystals and benders

The Laue crystals selected for the ID beamline are of the largest in use at synchrotron facilities. The 190 mm-wide, 14 mm-high and 2 mm-thick X-ray window of the crystal requires up to 50 N of force, or up to 5 N m of torque applied to the benders in order to effectively bend it to a ∼10 m radius. The PI M-111 micro-translation stage is used for bending force. Several different options for the benders were evaluated and, in the end, only high-strength spring steel AISI-1095 was deemed to deliver the required force. Fig. 3 shows the implementation of the benders, where the force is applied at the 84 mm position vector on each bender. The benders are 1.27 mm (0.05 inch) thick and 10 mm wide.

The high torque on the top of the crystal also creates high torque at the base. The base of the crystal is locked in place with holding springs/clamps (see Fig. 4). The original design, which used a circular spring leaf, was very stiff and, because the spring was connected with the crystal over a small contact area, it created stress points which were visible in the beam. It was also very difficult to align and tension properly.

This design was later replaced with a dynamic floating clamp design, where the base is held in place with a stainless-steel clamp which holds the base of the crystal over a large contact area. Every bolt holding the clamp to the base compresses two small Belleville disk springs to achieve up to 200 N total holding force. Each spring is set to work at ∼25% of its working load of 80 N. This design is performing extremely well; it firmly holds the base of the crystal in place and the holding position is independent of the crystal temperature
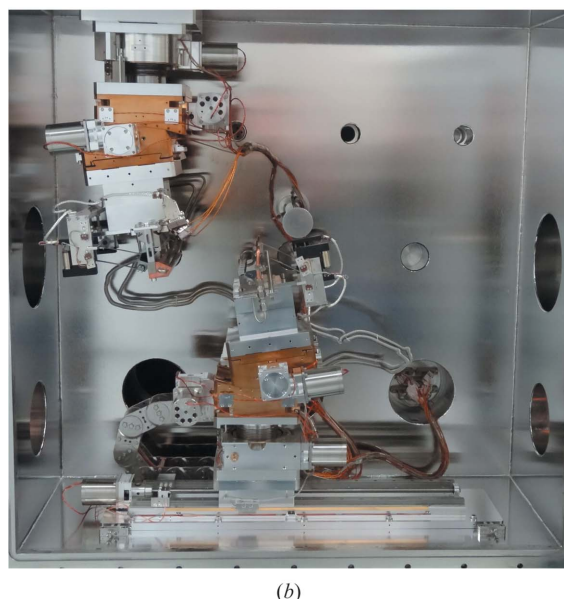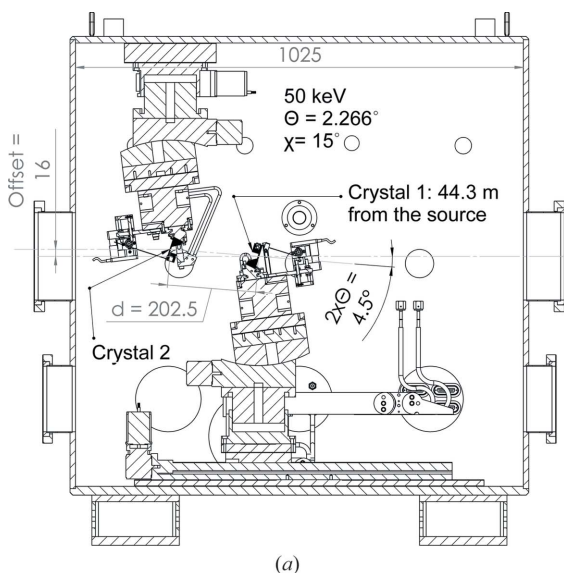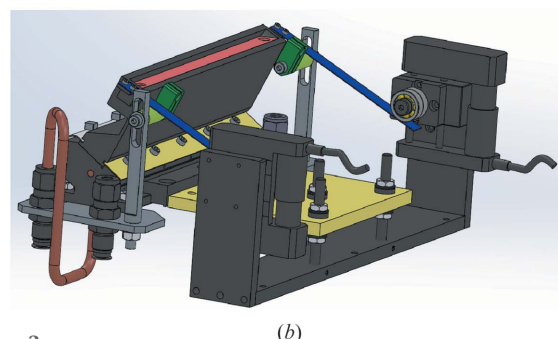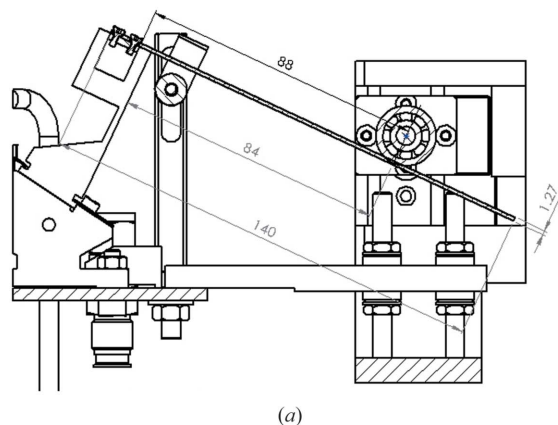
Figure 2
(*a*) CT monochromator schematic with crystals positioned for a 50 keV set-point and (*b*) an internal view. White beam is entering from the right. The crystal pair is made of silicon using (111)-type reflections. The asymmetry angle $\chi = 15°$ is the angle between the Bragg planes and the surface normal of the crystal.

as the springs can easily accommodate the expansion of the crystal as it heats up.

3. FEA study

Actual operating parameters of the monochromator, such as the crystals' bending radii, the position of the crystals in relation to the displacement of the benders and the resulting beam parameters (height, divergence), depend on monochromator component characteristics and may differ from the theoretical ideal model. For the first step in the monochromator operating point assessment, we attempted finite element analysis (FEA) of the complete crystal assembly,

Figure 3
(*a*) The first CT monochromator crystal and benders assembly drawing and (*b*) a three-dimensional model. White beam is entering from the right. The crystals have two 2×2 mm grooves at the base which are used for holding the crystal (using clamps) to a copper base which also provides the required cooling.

which includes clamps, crystals, bender support brackets and benders. As with any FEA of a complicated assembly, there is a probability of errors related to necessary model simplifications. We started with the FEA of all the individual components separately in a simple configuration (see Table 1 for parameters) to verify the FEA method and to confirm the theoretical material properties such as Young's modulus and Poisson's ratio.
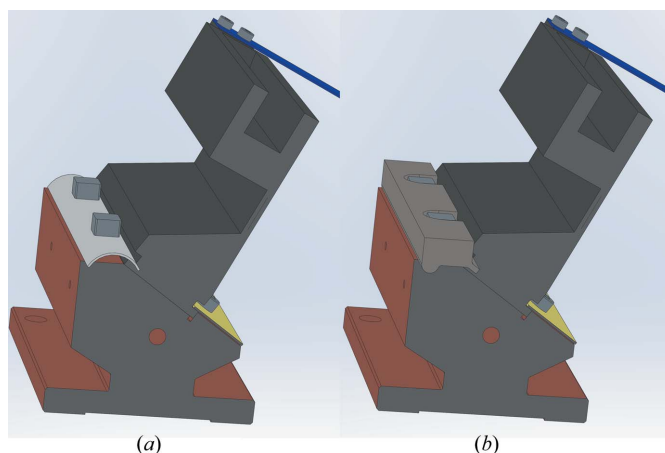
Figure 4
(*a*) Crystal base original leaf spring clamp and (*b*) the modified design.

Table 1
Mechanical properties of the bender and silicon materials used for FEA simulation.

	Benders	Bender support brackets	Crystal†
	AISI-1095	Mo	Si
Density (kg m^{-3})	7870	10220	2329
Poisson's ratio (a.u.)	0.29	0.38	0.262
Young's modulus (Pa)	1.8×10^{11}‡	3.3×10^{11}	1.69×10^{11}

† We assumed isotropic Poisson's ratio and Young's modulus for silicon. For a more detailed analysis they should be considered as anisotropic (Zhang *et al.*, 2014). ‡ The Young's modulus value of cold drawn AISI 1095 is 1.9×10^{11} to 2.1×10^{11} (https://www.azom.com/article.aspx?ArticleID=6561).

3.1. Benders and crystals parameters

For the bender material, we compared the supplier-provided material parameters with the measured values. The benders before installation in the monochromator were tested with a load cell to establish the force and displacement relationship. The same process was modeled using FEA (*ANSYS Workbench* 18.0) with theoretical material parameters and the results were compared. The experimental measurements showed slightly lower Young's modulus values than the theoretical model. This can be related to the method of attaching the benders to the support bracket and to potential material parameter changes caused by strain and heating during bender fabrication. To match the FEA results with those measured, the theoretical Young's modulus for the benders used for FEA was adjusted so the two methods converged (Table 1). For the silicon crystal, we assumed it has isotropic Poisson's ratio and Young's modulus in the simulation. The analysis presented here does not incorporate thermal effects, including thermal distortion of the crystal caused by heat bump and thermal expansion.

We attempted to use FEA to develop functions which, as a result, would connect the bending radius of the crystal with the applied force, torque and eventually with the motor displacement of the bender. FEA is also used to establish the safety factor with the nominal loads applied. The developed model provided a good approximate representation of the actual system, with an accuracy of 1–2 m for a ∼20 m bending radius point. In the next step, the FEA model was verified experimentally, which included measurement of the vertical beam divergence in the SOE-1 hutch in order to calculate the virtual focus of the second crystal. A set of those measurements at different energies and different bender displacement points can provide enough data points to calibrate the FEA model with higher accuracy, so it can be reliably used for estimating the required bender settings for a collimated beam at different energy points. One of the conclusions drawn was that the motor travel of the bender requires an accuracy of at least 10 µm to accurately set the crystals' bends.

As a result of the high temperatures and radiation inside the monochromator, the bender material degrades with time, which changes the bending radius of the crystal and alters the operating conditions of the monochromator. By measuring these changes over time and substituting modified values into the focusing and FEA model, it is relatively easy to define the creep rate of the material properties and to make the required corrections.

3.2. FEA model and results

Fig. 5 provides the main model dimensions and the force set-points used for the analysis and shows the calculated von Mises stress of the silicon crystal.

The ultimate tensile strength of monocrystalline silicon is about 350 MPa, hence, in the region of interest (ROI) (X-ray window), we can observe a safety factor of around seven times with a total 100 N force applied to the benders. However, one can see that the stress may reach values very close to the ultimate tensile strength in the area where the bender-holding brackets are attached to the crystal if a force of 100 N is applied like in the example above. The vector deformation data are used in the next step to define the bending radius of the crystal.
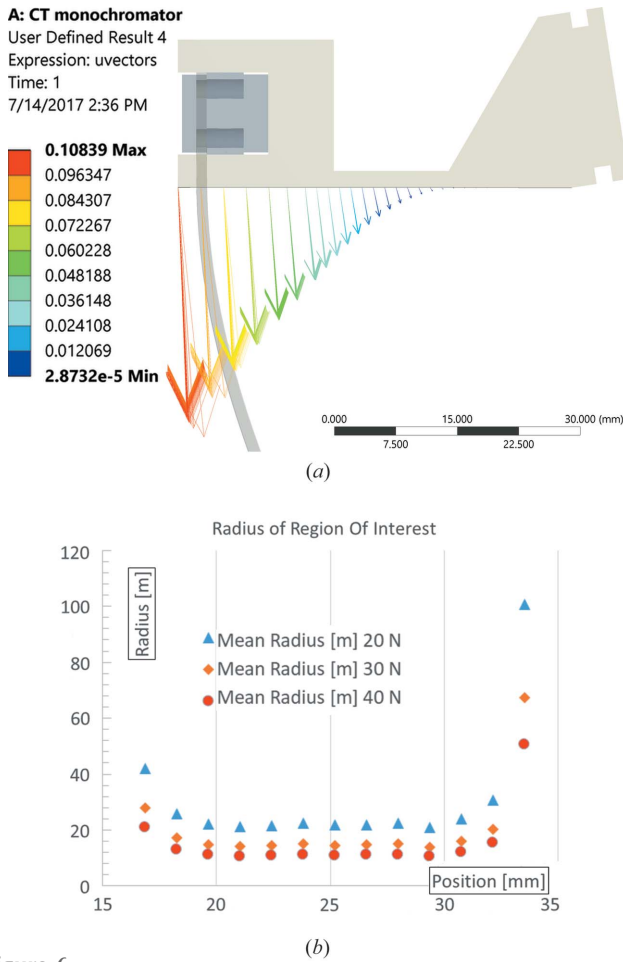
3.3. Bending radius estimates

Further FEA studies (see Fig. 6) provide the vector deformation matrix at several different loads (10 N, 15 N and 20 N) applied to each bender. These data are used to estimate the bending radius of the crystal's X-ray window. To make this correlation, we have used the circumscribed circle method, the results of which are shown in Fig. 6(*b*). The analysis shows that the radius is constant for the ROI (X-ray window). Based on
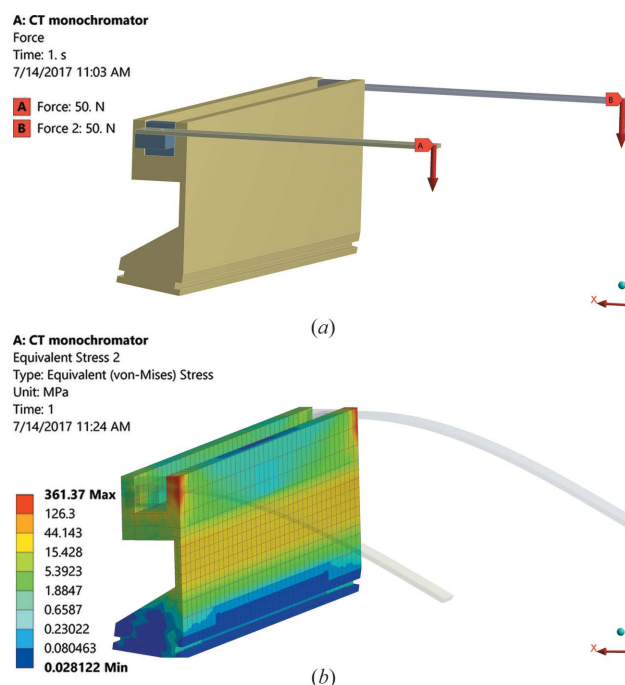
Figure 5
(*a*) Three-dimensional model of the Si crystal. The crystal is 190 mm wide and 55 mm high with the X-ray window 14 mm high and 2 mm thick. The applied force is 50 N at the 84 mm position vector on each bender for a total of 100 N. The benders are 1.27 mm (0.05 inch) thick and 10 mm wide. We assume the base of the crystal is fixed. (*b*) Equivalent von Mises stress with a total of 100 N force applied.

A: CT monochromator
User Defined Result 4
Expression: uvectors
Time: 1
7/14/2017 2:36 PM

0.10839 Max
0.096347
0.084307
0.072267
0.060228
0.048188
0.036148
0.024108
0.012069
2.8732e-5 Min

0.000   15.000   30.000 (mm)
7.500   22.500

(a)

Radius of Region Of Interest

▲ Mean Radius [m] 20 N
◆ Mean Radius [m] 30 N
● Mean Radius [m] 40 N

(b)

Figure 6
(a) Vector deformation of the ROI of the silicon crystal with a total force of 100 N applied and (b) the radius of the ROI with 10, 15 and 20 N applied on each bender.

Table 2
Theoretical correlation between the bender displacement, force and torque applied to the crystal and estimated bending radius of the window based on the FEA study.

Bender displacement (mm)	Total force (N)	Total torque (N m)†	Estimated bending radius (m)
5.0	15.5	1.3	31.0
7.5	23	1.9	20.7
10	31	2.5	15.5
14	43	3.6	11.1

† Total indicates force and torque are applied with two benders.

chromator operation is to expand the beam (increase the vertical divergence) and increase the reflectivity as much as possible by bending the first crystal to the safe limit and then adjusting the bend of the second crystal so that an elemental ray should make the same angle with the Bragg planes at both crystals. This will satisfy the condition for a non-dispersive crystal pair at all energies. In this case, the real source for the second crystal (p_2), which is also the virtual focus of the first crystal (q_1), is on the Rowland circle, $p_2 = p_{02}$. Sometimes the goal is to generate a parallel (collimated) beam in the SOE-1 hutch; in this case, the real source for the second crystal (p_2), which is also the virtual focus of the first crystal (q_1), is the mid-point of the chord inside the Rowland circle, $p_2 = p_{02}/2$. The focal distances (see Fig. 7) p (source-to-crystal) and q [crystal-to-image (focus)] are related for each crystal by (Chukhovskii & Krisch, 1992; Suortti et al., 1994)

$$q = q_0/(2 - p_0/p),$$
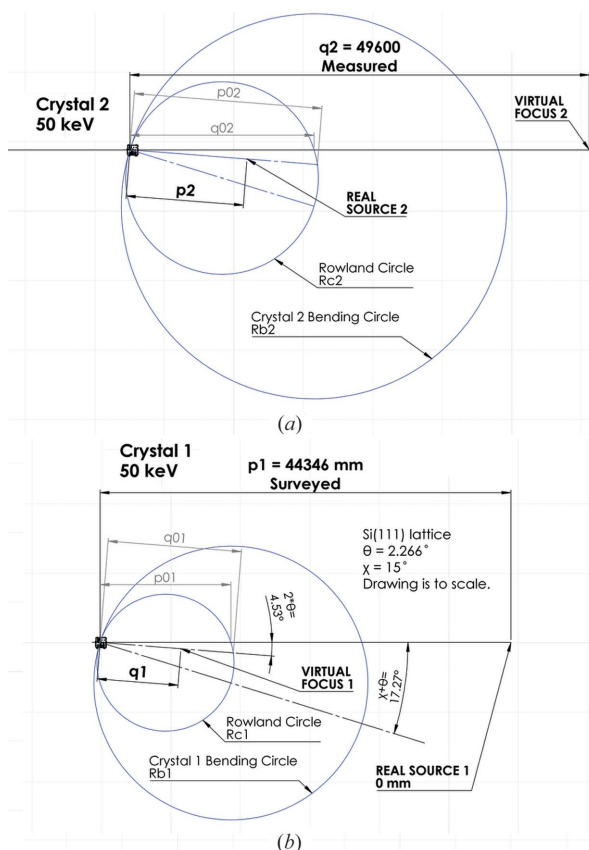
which can be rewritten as

$$p = p_0/(2 - q_0/q).$$

The source-to-first-crystal distance, p_1, and the first-crystal-to-second-crystal distance, d, are confirmed by survey and by the X stage position of the first crystal. Both p_1 and d need to be updated for each energy point as the first crystal travels along the beam in order to keep the exit beam at a fixed vertical displacement. All other points, including p_0 and q_0 (for both crystals), as well as the focus (image) point q_1, of the first crystal are calculated from the equations above. Points p_2 and q_1 are connected by the equation

$$p_2 = q_1 + d,$$

where d is the distance between the crystals for any given energy point. Point q_2, the distance from the second crystal to the virtual source, can be defined by measuring the divergence of the beam in SOE-1. By combining these relations and the results of the measurements, we can develop a complete focusing model that can help us to evaluate the required bending radius of the second crystal based on the bending radius of the first crystal.

5. Beam-focusing model

Fig. 7 shows the relative position of the source and image/focus for both crystals. This theoretical model assumes 10 mm

this analysis, we can correlate the bending radius of the crystal with force, torque and the bender displacement:

$$R = 39.4/\tau = 486/F = 154.9/df \text{ [m]},$$

where R (m) is the bending radius of the crystal, τ (N m) is the total torque (from two benders), F (N) is the total force applied (from two benders) and df (mm) is the displacement/deflection of the single bender from the neutral position (when the crystal is unbent).

Table 2 provides typical values of the force, torque and the theoretical bending radius for selected bender displacement points. The relatively thick and wide crystal used in the CT monochromator requires significant bending torque to deliver a bending radius below 20 m.

4. Beam-focusing model development

In this section, we apply the calculated parameters in order to estimate the virtual foci of the first (q_1) and the second (q_2) crystal in the monochromator and develop a full focusing model for DCLM. We assume focusing by an ideal, cylindrically bent thin crystal and we neglect the deformations due to the heating up of the crystal. The objective of the mono-

Figure 7
To-scale drawing of the source, focus and bending radius at 50 keV point for (a) crystal 2 and (b) crystal 1; the beam is traveling right to left. The surveyed distance between the crystals is $d = 202.5$ mm at 50 keV (see Fig. 2). Source 1 (origin at 0 mm) is defined as the middle of the wiggler.

Table 3
Summary of beam parameters at different energy points.

The position of the second crystal is fixed at 44.55 m from the source. Beam offset is 16 mm. Asymmetry angle $\chi = 15°$. We estimate $Rb_1 = 19.7$ m and $Rb_2 = 20.8$ m.

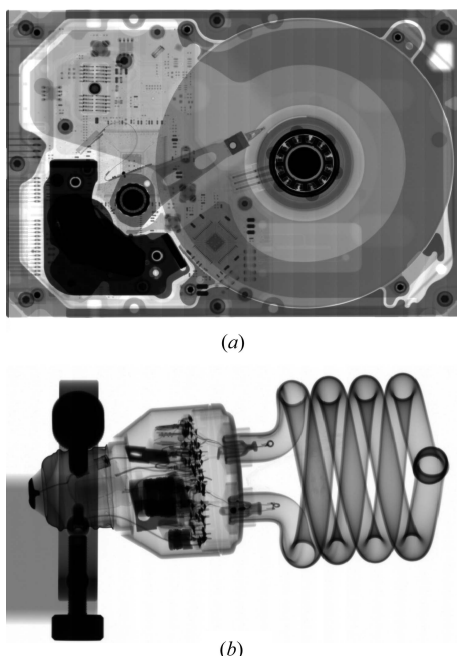| Energy (keV)	p_1 (m)	q_1 (m)	p_2 (m)	q_2 (m)	d (m)	Vertical divergence angle (°)
31.3	44.4	12.23	12.36	49.1	0.1	9.3×10^{-3}
50	44.3	12.2	12.4	49.6	0.2	9.6×10^{-3}
124.8	44.0	12.18	12.68	53.7	0.5	9.6×10^{-3}

heat-load is smaller when compared with the first crystal. After two years of operation, the spring constant of the bender on the first crystal must have degraded and we can estimate the equivalent (effective) displacement on the benders for crystal 1 at around ~8.1 mm, rather than 10 mm. This finding will be assessed during the next maintenance of the monochromator.

To complete the characterization of the monochromator, we recorded the three-dimensional intensity distribution map and measured the full width at half-maximum (FWHM), see Fig. 8.
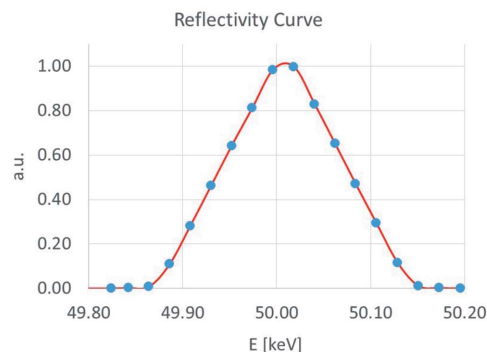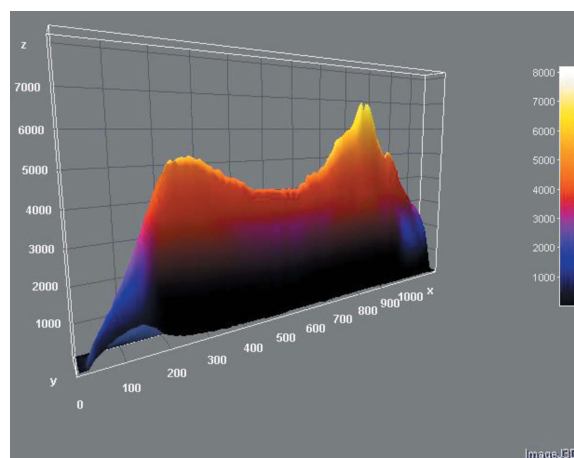
Figure 8
The intensity distribution of the monochromatic beam at 50 keV, recorded with a Hamamatsu C9252DK-14 flat-panel detector in SOE-1 (top). The x axis corresponds to width, the y axis to the height of the beam and the z axis presents intensity. The reflectivity curve as recorded with the pin-point TN31014 ion chamber and 0.3 mm (V) slit collimator at 50 keV with $Rb_2 = 20.8$ m and $Rb_1 = 19.7$ m, FWHM = 6.57×10^{-3} degree (0.11475 mrad), or 145 eV or 0.29% (bottom).

displacement of the bender on crystal 1 and 7.5 mm displacement on crystal 2. Those displacement points were selected during the commissioning of the monochromator in 2014, as this combination provided the most uniform and bright beam. The energy used in the example below is set at 50 keV. The position of the first crystal is at 44.35 m from the source. Beam offset is 16 mm. To obtain a monochromatic beam, the $p_2 = p_{02}$ criterion must be met. To obtain a collimated beam, the $p_2 = p_{02}/2$ criterion must be met.

Next, we compared this theoretical model with the experimental data acquired in 2017. The position of the focus/image (q_2) for crystal 2 was established by the beam height measurements at three different distances inside the SOE-1 hutch. We found the beam diverging, hence our model shows that $p_2 > p_{02}/2$. Table 3 shows measured q_2, surveyed p_1 and d parameters for three energy points for which the beam divergence was measured. When combining surveyed (p_1, d) and measured (q_2) dimensions, we can estimate the ratio of Rb_1:Rb_2 for any given energy and we can compare this ratio with the theoretical values from Table 2. For the current (in 2018) operating point, we can conclude that the actual bending radius for the first crystal is larger than the theoretical one. We also assumed that the radius of the second crystal did not change as much, as the initial bender displacement and the

Tomasz W. Wysokinski et al. • High-power-load DCLM monochromator

Figure 9
(a) Radiograph (100 μm resolution) of a 3.5 inch hard-drive and (b) a fluorescent bulb, imaged at 70 keV with a 3.5 mm Cu filter used to remove the soft X-rays, total dose 0.3 mGy. The images were taken as a step, shoot and stitch method using a Hamamatsu C9252DK-14 flat-panel detector.

6. Hard X-ray imaging examples

The DCLM installed on the 05ID-2 beamline is the primary source of monochromatic radiation used for advanced imaging and X-ray therapy experiments at BMIT. Ongoing core research programs include: bone/cartilage imaging, cardiovascular and lung imaging, cancer therapy and medical device and scaffold imaging as well as the introduction of new imaging methods (Wysokinski, Ianowski *et al.*, 2016).

The main attribute of this monochromator is the wide field of view and high energy range available (requirements perfectly suited for imaging large and dense objects). Fig. 9 shows an example of non-destructive imaging of a hard drive and a fluorescent bulb at 70 keV.

These images confirm that this monochromator provides a high-quality wide beam that can penetrate thick and dense objects. The final products are high-quality and high-resolution images with a relatively low dose required.

7. Conclusions

This paper describes the design requirements and operational parameters for the high-power-load monochromator that has been constructed for CT studies at the BMIT facility. The monochromator operates at energies from 25 keV to 150 keV, and the crystals are 190 mm wide. The X-ray window is 14 mm high and 2 mm thick. The beam intensity is between 10^{12} and 10^{13} photons s^{-1} mm^{-2} under typical operating conditions, which is sufficient for studies of medium-sized animals with a resolution down to 4 μm. An FEA study of the complete crystal-bending assembly was attempted in order to develop a full focusing model of the monochromator. The analysis provides theoretical functions which can relate the bending radius of the silicon crystal to the bender displacement. The FEA model has to be verified experimentally by measurements of the beam divergence to calibrate the model. A set of these measurements at different bender displacement points can provide enough data so that the FEA model can be reliably used for finding monochromatic or collimated beam setpoints at different energy settings. One of the conclusions of this analysis is that the bender motor travel requires an accuracy of at least 10 μm to accurately set the monochromator to the desired operating set-point. With the estimated effective displacement on the benders of 8.2 mm and 7.5 mm, the measured FWHM of the spectral bandwidth at 50 keV is 0.29%. An improved design of the holding springs, which is one part of the development, makes the monochromator quite insensitive to vibrations. It can operate with a small turbo pump attached and pumping for medium-resolution imaging at a pixel size of 20–50 μm without vibration related artifacts. Due to high power loads, the system experiences high out-gassing, and therefore a proper filter set to control the vacuum level, protect the crystal and to reduce thermal drift is required.

References

Chukhovskii, F. N. & Krisch, M. (1992). *J. Appl. Cryst.* **25**, 211–213.
Renier, M., Rack, A., Valade, J. P., Boller, E., Bernard, P. & Tafforeau, P. (2016). *Aip Conf. Proc.* **1741**, 040025.
Stevenson, A. W., Crosbie, J. C., Hall, C. J., Häusermann, D., Livingstone, J. & Lye, J. E. (2017). *J. Synchrotron Rad.* **24**, 110–141.
Suortti, P., Buslaps, T., Honkimäki, V., Kretzschmer, M., Renier, M. & Shukla, A. (2001). *Z. Phys. Chem.* **215**, 1419.
Suortti, P., Fiedler, S., Bravin, A., Brochard, T., Mattenet, M., Renier, M., Spanne, P., Thomlinson, W., Charvet, A. M., Elleaume, H., Schulze-Briese, C. & Thompson, A. C. (2000). *J. Synchrotron Rad.* **7**, 340–347.
Suortti, P., Lienert, U. & Schulze, C. (1994). *Nucl. Instrum. Methods Phys. Res. A*, **338**, 27–32.
Wysokinski, T. W., Chapman, D., Adams, G., Renier, M., Suortti, P. & Thomlinson, W. (2007). *Nucl. Instrum. Methods Phys. Res. A*, **582**, 73–76.

Wysokinski, T. W., Chapman, D., Adams, G., Renier, M., Suortti, P. & Thomlinson, W. (2015). *Nucl. Instrum. Methods Phys. Res. A*, **775**, 1–4.

Wysokinski, T. W., Chapman, L. D., Miller, D., Belev, G., Lin, L. D., Adam, M., Wurtz, W. & Dallin, L. (2016). *Aip Conf. Proc.* **1741**, 020026.

Wysokinski, T. W., Ianowski, J. P., Luan, X., Belev, G., Miller, D., Webb, M. A., Zhu, N. & Chapman, D. (2016). *Phys. Med.* **32**, 1753–1758.

Zhang, L., Barrett, R., Cloetens, P., Detlefs, C. & Sanchez del Rio, M. (2014). *J. Synchrotron Rad.* **21**, 507–517.